Applied Physics Letters

RESEARCH ARTICLE | SEPTEMBER 18 2020

The effect of finite sample thickness in scanning ion conductance microscopy stiffness measurements

Johannes Rheinlaender ; Tilman E. Schäffer

Appl. Phys. Lett. 117, 113701 (2020)
https://doi.org/10.1063/5.0024863

AIP Publishing

Applied Physics Letters ARTICLE scitation.org/journal/apl

The effect of finite sample thickness in scanning ion conductance microscopy stiffness measurements

Cite as: Appl. Phys. Lett. **117**, 113701 (2020); doi: 10.1063/5.0024863
Submitted: 12 August 2020 · Accepted: 2 September 2020 ·
Published Online: 18 September 2020

View Online Export Citation CrossMark

Johannes Rheinlaender[a] and Tilman E. Schäffer[a]

AFFILIATIONS

Institute of Applied Physics, University of Tübingen, Auf der Morgenstelle 10, 72076 Tübingen, Germany

[a]Authors to whom correspondence should be addressed: johannes.rheinlaender@uni-tuebingen.de and tilman.schaeffer@uni-tuebingen.de

ABSTRACT

Investigating the mechanical properties of soft biological samples on the single-cell level is of great interest as cell mechanics play a central role in many physiological processes in health and disease. Scanning ion conductance microscopy (SICM) is an emerging technique for measuring cell stiffness on the micro- and nanometer scale in a non-contact fashion. However, as SICM stiffness measurements are based on a localized deformation of the sample, they are affected by the thickness of the sample. We found experimentally and numerically that the apparent stiffness of a thin sample is overestimated. We present a straightforward correction method to account for this effect and derive a thickness-dependent, multiplicative correction factor, which we apply to SICM stiffness mapping of living cells. The correction method allows us to quantitatively measure the stiffness of thin samples with SICM and is, therefore, essential for the comprehensive application of SICM to nanomechanical measurements.

Measuring the mechanical properties of living cells and tissue is of high interest because mechanics play a pivotal role both in normal cell function[1,2] and in disease.[3,4] Scanning probe microscopy techniques such as atomic force microscopy[5] (AFM) are well-suited for such measurements,[6] since they allow us to spatially resolve the mechanical stiffness on the micro- and nanometer scale.[7] Recently, scanning ion conductance microscopy[8] (SICM) has been used for mechanical measurements[9] [Fig. 1(a)] and even mapping sample stiffness.[10]

For both AFM and SICM, measuring sample stiffness is based on locally indenting the sample. For AFM, it is well known that the sample stiffness is significantly overestimated on thin samples[11] and various correction models have been developed for different tip geometries, including spherical,[12,13] conical,[14,15] or flat-ended cylindrical tips.[16] For SICM, however, the effect of the finite sample thickness on the measured sample stiffness [Fig. 1(b)] has never been investigated yet.

In the present study, we show that the finite sample thickness does indeed result in a significant overestimation of the sample stiffness when measured with SICM. We developed a correction method based on finite element modelling (FEM) to compensate for this effect. Finally, we apply the correction method to a stiffness mapping measurement on living cells.

We used a conventional SICM setup, where an electrolyte-filled nanopipette is moved with respect to the sample in x-, y-, and z-directions using piezo scanners while the ion current I through the

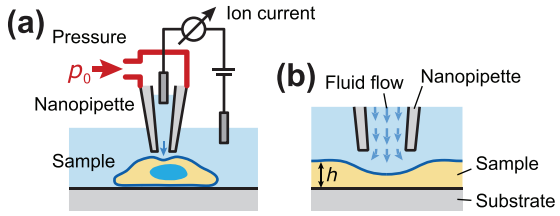

FIG. 1. Stiffness measurements with SICM. (a) Schematic SICM setup for measuring sample stiffness. Applying a constant pressure p_0 to the upper end of the nanopipette induces a microfluidic flow. The resulting deformation of an elastic sample is detected using the ion current through the nanopipette. (b) Deformation of a thin elastic sample of height h supported by a rigid substrate.

nanopipette is recorded. Additionally, a constant pressure p_0 (150 kPa in Fig. 2 and 10 kPa in Fig. 4, adapted to the expected stiffness of the respective sample) is applied to the upper end of the capillary, resulting in a microfluidic flow through the nanopipette.[9,10,17] Ion current vs distance (*IZ*) curves were recorded over different regions of the sample. The local sample height, z, was determined as the vertical pipette position where the current decreased to 99% of the maximum current (where almost no forces act on the sample); the local apparent sample "stiffness" in terms of Young's modulus, E_{app}, was determined from the average slope of the *IZ*-curve between the points corresponding to 98% and 99% of the maximum current, as described previously.[10] The nanopipettes were fabricated from borosilicate glass capillaries (1B100F-4, World Precision Instruments Inc., Sarasota, FL) using a CO_2-laser-based micropipette puller (P-2000, Sutter Instruments, Novato, CA). The nanopipettes used here had a typical inner cone angle of $\alpha = 4°$ and a ratio of outer to inner opening radius of $r_o/r_i = 1.5$. The inner opening radius was determined as $r_i = 220$ nm (Fig. 2) or $r_i = 110$ nm (Fig. 4) by fitting the *IZ*-curves.[18] We chose large or small pipettes to trade-off between a small ratio of sample thickness to pipette radius (large pipettes, Fig. 2) and sufficient imaging resolution[19] (small pipettes, Fig. 4). Topography images were background corrected using a first-order plane fit so that the surface of the cell culture dish is at $z = 0$.

Elastomer wedges were made from Sylgard 527 (Dow Corning Corporation, Auburn, MI), one of the softest silicone elastomers commercially available. The elastomer was mixed at the nominal mixing ratio of 1 : 1, deposited as small drops on glass cover slips, and cured at 100 °C for 3.5 h. The cover slips were then glued into culture dishes and imaged with SICM at room temperature in phosphate-buffered saline (PBS) solution. The actual stiffness of the used elastomer sample was measured with SICM on a thick region as $E = 70$ kPa. This value agreed, within an error, with a measurement of the same elastomer using AFM (MFP3D-BIO, Asylum Research, Santa Barbara, CA) using a sphere-tip cantilever with a 370 nm tip radius (CONT-S-SPL, NanoWorld, Neuchatel, Switzerland), giving 80 ± 10 kPa. For imaging living cells, human platelets were isolated as described previously,[19] allowed to adhere and spread on a culture dish (Cellstar, 627160, Greiner Bio-One, Kremsmünster, Austria) surface for 10 min, activated with 0.5 U/ml thrombin, and imaged at room temperature in Tyrodes buffer.

FEM calculations were performed as described previously.[10] Briefly, the nanopipette was modeled as conical with inner opening radius r_i, outer opening radius r_o, and inner half cone angle α. The laminar fluid flow through the nanopipette driven by a constant pressure p_0 at the upper end of the nanopipette, the resulting deformation of a flat, elastic sample, and the ion current I through the nanopipette considering the deformed geometry were calculated by FEM calculations [see Fig. 3(a)] using COMSOL Multiphysics (COMSOL AB). The sample was modeled as a linear-elastic material with Young's modulus E, Poisson's ratio ν between 0.3 and 0.499 (modelling an incompressible sample with $\nu = 0.5$ was not possible for numerical reasons), and as either sticking to or sliding on the underlying rigid substrate (see Table I). The sample thickness was modelled between $h = 0.5\,r_i$ and $10\,r_i$; the lateral dimension of the model was set to $20\,r_i$ to avoid edge effects. The assumption of a linear-elastic material is justified here as the sample deformation, δ,[10] was generally much smaller than the sample thickness (typically $\delta/h < 0.1$).

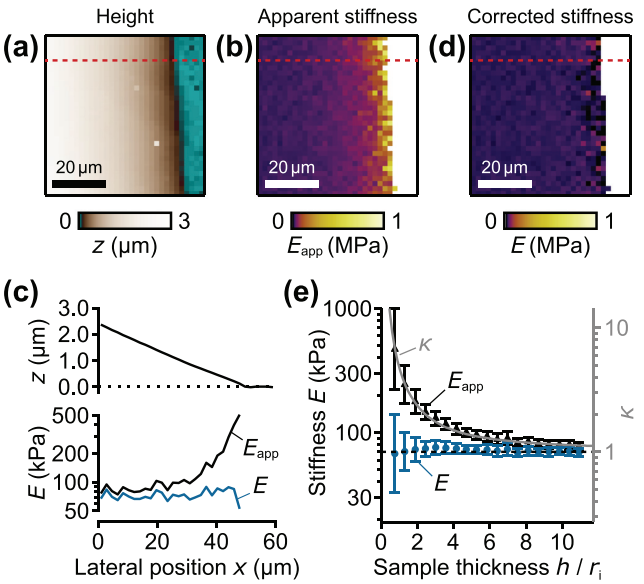

FIG. 2. Experimental verification of the thickness effect. (a) Topography image and (b) map of apparent stiffness E_{app} of an elastomer wedge sample. (c) Profile of topography (top) and stiffness (bottom) along the red dashed lines in the images. (d) Map of corrected stiffness $E = (1/\kappa)\,E_{app}$ with κ from Eq. (1). (e) Apparent stiffness E_{app} (black triangles) and corrected stiffness E (blue circles) as a function of elastomer sample thickness. The dashed horizontal line indicates the estimated actual elastomer stiffness. The gray trace shows the thickness effect factor κ as predicted by Eq. (1). Error bars represent geometrical standard deviation.

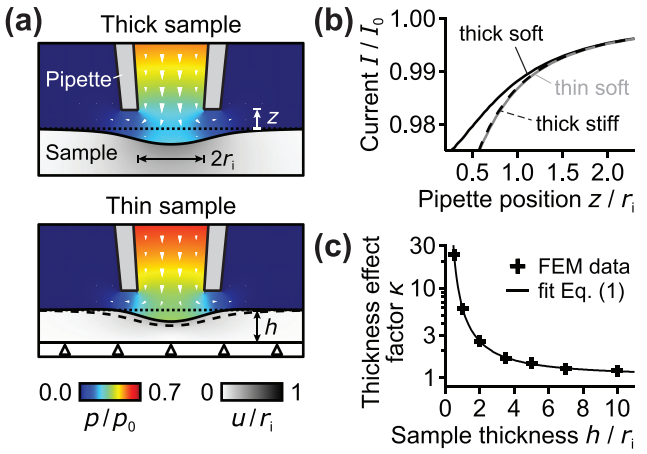

FIG. 3. Numerical model. (a) FEM calculations of fluid flow (arrows), pressure (color scale), and sample deformation (gray scale) for a soft thick sample (top panel) and a soft thin sample on a rigid substrate (bottom panel). The deformed sample surface of the thick sample is outlined as a dashed curve in the bottom panel. (b) Ion current I vs vertical pipette position z for a thick soft (solid black trace), a thin soft (gray trace), and a thick stiff sample (dashed black trace). I_0 denotes the maximum ion current far away from the sample. (c) Thickness effect factor κ as a function of sample thickness h and fit of Eq. (1) with a, b, and c as free fit parameters. The parameters for the shown calculations are $z = 0.6\,r_i$ (corresponds to approximately 98% ion current), ratio of the outer to inner pipette opening radius $r_o/r_i = 1.5$, inner half cone angle $\alpha = 4°$, sample stiffness $E = 1.0\,p_0$ ("soft") or $5.0\,p_0$ ("stiff"), Poisson's ratio $\nu = 0.499$, and $h = 1.0\,r_i$ ("thin") or $10\,r_i$ ("thick").

TABLE I. Parameters *a*, *b*, and *c* in the thickness effect interpolation function, Eq. (1), for different sample Poisson's ratios ν and for the two cases of the sample either sticking or sliding on the underlying rigid substrate, determined by fitting Eq. (1) to the respective numerical data [see supplementary material Fig. S1(c)].

	Sample sticking			Sample sliding		
Sample Poisson's ratio ν	*a*	*b*	*c*	*a*	*b*	*c*
0.3	0.569	1.92	2.60	0.319	1.36	3.24
0.4	0.731	2.35	1.91			
0.45	0.975	2.66	1.40			
0.499	1.462	3.30	0.66			

Data processing and analysis were carried out with IGOR Pro 6 (Wavemetrics, Portland, OR). Averages were stated as geometric mean ⁎ geometric standard deviation.

To identify whether stiffness measurements with SICM are affected by the sample thickness, we investigated a wedge-shaped elastomer sample (Fig. 2) of well-known, uniform stiffness (see above). From the topography image [Fig. 2(a)] and apparent stiffness [Fig. 2(b)] images as well as in the respective profiles [Fig. 2(c), black traces], it can be seen that the apparent stiffness indeed notably increases on the thin region of the sample, here by a factor of up to ≈5. Accordingly, the apparent stiffness from Fig. 2(b) is highly correlated with the sample thickness [Fig. 2(e), black triangles].

For numerically investigating the thickness effect with FEM, first, the influence of the sample thickness was visualized for two soft samples of identical stiffness but different thicknesses [Fig. 3(a)]. Compared to the thick sample [Fig. 3(a), top panel], the indentation for the thin sample [Fig. 3(a), bottom panel] is smaller. The thin sample, therefore, appears stiffer than the thick sample. Second, the influence of the sample thickness on *IZ*-curves was investigated [Fig. 3(b)]. Compared to the *IZ*-curve on the thick soft sample (solid black trace), the *IZ*-curve on the thin soft sample (gray trace) is much steeper. Interestingly, for every *IZ*-curve on a thin soft sample, one can identify an *IZ*-curve for a thick but stiffer sample, which matches the *IZ*-curve on the thin soft sample. Here, the *IZ*-curve on the thin sample with thickness $h = 1.0\,r_i$ (gray trace) matches that on a thick ($h = 10\,r_i$) and about fivefold stiffer sample [Fig. 3(b), dashed black trace]. This factor is independent of the absolute sample stiffness and, thus, of indentation depth [see supplementary material Fig. S1(a) and S1(b)], but it is thickness-dependent. By comparing *IZ*-curves for different stiffness and thickness values [see supplementary material Fig. S1(b) and S1(c) for details], we determined the thickness effect factor $\kappa = E_{app}/E$ as a function of sample thickness h [Fig. 3(c), markers], analogue to the literature.[20,21] κ depends only weakly (within 10%) on the pipette wall thickness or cone angle (not shown). For convenience, the FEM data can be interpolated well (within typically 1%) using an empirical interpolation function,

$$\kappa(h) = \exp\left(a\frac{r_i}{h}\right) + b\frac{r_i}{h}\left[1 - \exp\left(-c\frac{r_i}{h}\right)\right] \quad (1)$$

[Fig. 3(c), trace], adapted from the thickness effect factor for flat-ended cylindrical indenters.[21] The dimensionless parameters *a*, *b*, and *c* in Eq. (1) are tabulated in Table I for different Poisson's ratios and for the two cases where the sample either sticks or slides on the underlying rigid substrate. Generally, κ is larger for a larger Poisson's ratio and when the sample sticks as compared to when it slides on the underlying rigid substrate (see Table I). For a sample sliding on the substrate, κ does not depend on Poisson's ratio (see Table I). The corrected stiffness can then be obtained by multiplying the apparent stiffness with a correction factor, $1/\kappa$, which is the inverse of the thickness effect factor κ.

To verify the numerical results, we again consider the wedge-shaped elastomer sample (Fig. 2). When accounting for the finite sample thickness (using $\nu = 0.45$, as the elastomer is nearly incompressible,[22,23] and sample sticking to the rigid substrate[24]), the corrected stiffness $E = (1/\kappa)\,E_{app}$ is uniform across the whole sample [Fig. 2(d)] and does not increase on thin regions of the sample [Fig. 2(c), blue trace]. Accordingly, the corrected stiffness is constant [Fig. 2(e), blue circles] and well matches the actual stiffness of 70 kPa as estimated from SICM data on thick regions (see above). Consequently, the measured thickness effect factor κ, determined from the experimental data as $\kappa = E_{app}/70$ kPa, is well predicted by Eq. (1) [Fig. 2(e), gray trace].

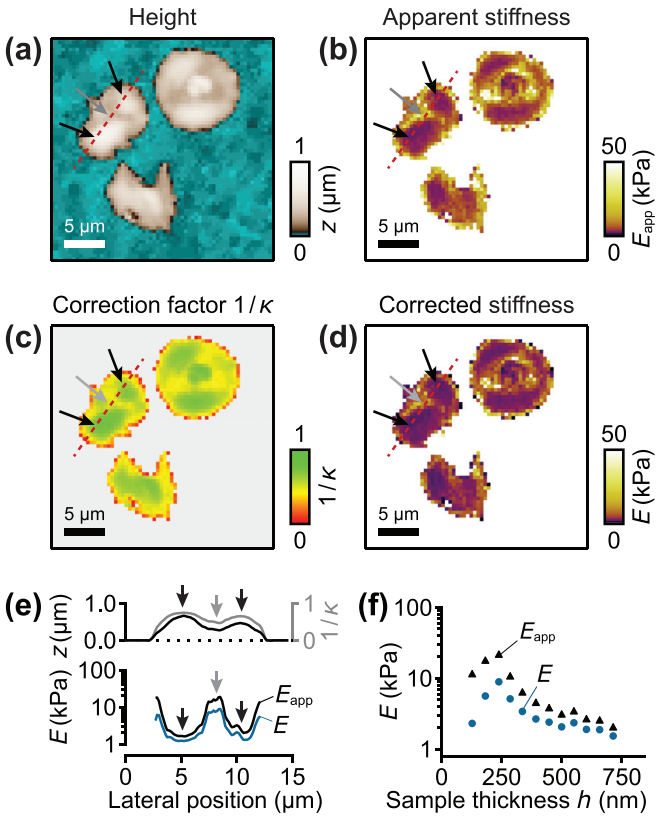

FIG. 4. Application of the thickness effect correction to the SICM stiffness measurement of living platelets. (a) Topography image and (b) map of apparent stiffness E_{app} of platelets adhered to a culture dish as an example for a thin elastic sample supported by a rigid substrate. (c) Map of stiffness correction factor $1/\kappa$ and (d) map of corrected stiffness $E = (1/\kappa)\,E_{app}$. (e) Profiles of topography and stiffness correction factor $1/\kappa$ (top) and apparent and corrected stiffness (bottom) along the red dashed lines in the images. (f) Apparent stiffness E_{app} (black triangles) and corrected stiffness E (blue circles) as a function of sample thickness.

To demonstrate SICM stiffness measurements of a thin, biologically relevant sample, living platelets adherent to a culture dish surface were imaged using SICM stiffness mapping (Fig. 4). The topography image [Fig. 4(a)] and map of apparent stiffness [Fig. 4(b)] show local variations in height and stiffness, respectively. Thick regions of the cells typically exhibit low stiffness (black arrows) and *vice versa* (gray arrows), as easily seen in the profiles [Fig. 4(e), black traces]. This results in a significant negative correlation between the cell stiffness and thickness [Fig. 4(f), black triangles]. When applying the stiffness correction here (using $\nu = 0.499$ and sample sticking to the rigid substrate as is usually assumed for living cells[12–15,25]), thick regions of the cells [Fig. 4(a), black arrows] have a correction factor $1/\kappa$ close to 1 [Fig. 4(c), black arrows] and are, thus, not affected by the correction, but thinner regions [Fig. 4(a), gray arrow] have a correction factor lower than 1 [Fig. 4(c), gray arrow]. The corrected stiffness [Fig. 4(d)] in thin regions is, therefore, lower than the apparent stiffness [Fig. 4(b)]. However, the relative differences in the stiffness map remain similar, since most thick regions of these living platelets are inherently softer than thin ones, visible also in the profiles [Fig. 4(e)]. There is still a negative but weaker correlation between corrected stiffness and thickness [Fig. 4(f), blue circles]. Compared to the apparent stiffness, the corrected stiffness is significantly smaller, here by about a factor of two with an average of 3.9⁎2.5 kPa as compared to an average apparent stiffness of 7.9⁎2.8 kPa.

The effect of the sample thickness on mechanical measurements is already well-studied for AFM, where, in the case of spherical/conical tips, the thickness effect depends in a complicated way on the indentation depth and thus (given a constant force) on the sample stiffness.[12–15,25] Since the thickness effect factor in SICM for linear elastic samples is independent of the indentation depth and sample stiffness (see supplementary material Figs. S1 and S2), a SICM stiffness measurement is conceptually similar to a flat-ended cylindrical indenter penetrating a thin elastic sample, a system already extensively studied in the literature beginning with Hayes *et al.*[20] The functional form of the thickness effect factor $\kappa(h)$ obtained by Hayes *et al.* is similar to that obtained here for SICM for an indenter radius of $a \approx 1.4\, r_i$ (not shown), indicating that the SICM pipette is comparable to a flat-ended cylindrical indenter of similar radius. Therefore, many aspects already studied in the literature for a flat-ended cylindrical indenter, such as the effects of large deformations,[26] friction between sample and substrate or indenter,[27] layered materials,[28] or viscoelasticity,[21,29,30] might be transferable to SICM likewise. For example, for a flat-ended cylindrical indenter, the thickness effect is also independent of the Poisson ratio when the sample is sliding on the substrate.[28] Recently, SICM was also used to measure the sample stiffness by van der Waals forces,[31,32] where the effect of the sample thickness should be equivalent to that for a flat-ended cylindrical indenter with a contact radius equal to the outer (instead of the inner) pipette opening radius.

Another aspect affecting the stiffness measurement in SICM is the local sample slope.[33] Recently, Swiatlowska *et al.*[34] introduced an approximate correction method based on a model by Thatenhorst *et al.*[33] predicting that the stiffness would be underestimated by a factor approaching the cosine of the slope angle. However, the samples in this study were relatively flat. For example, the elastomer sample (Fig. 2) has a slope angle of less than 3°, which would result in an underestimation of the stiffness by less than 1%.

In summary, we have shown in this study that the finite thickness of thin samples can have a notable influence on the measured stiffness in SICM measurements as demonstrated by calculations using FEM and experiments on elastomer and living cell samples. We present a straightforward correction method based on a thickness-dependent, multiplicative correction factor, which applies likewise to all SICM stiffness measurement procedures regardless of whether they are based on measuring pipette displacement,[9] distance between different ion current levels,[17] or slope of the *IZ*-curve.[10] Accordingly, the correction method can be applied to all these procedures and will, therefore, be of great benefit for all nanomechanical measurements with SICM.[35]

See the supplementary material for the determination of the thickness effect factor from FEM data and the experimental validation that the thickness effect is independent of sample deformation.

We thank Jan Seifert and Hendrik von Eysmondt for discussion and assistance in platelet preparation. We thank Asylum Research for technical support. This work was funded by the Deutsche Forschungsgemeinschaft (DFG, German Research Foundation)—Projektnummer 374031971 – TRR 240.

DATA AVAILABILITY

The data that support the findings of this study are available from the corresponding author upon reasonable request.

REFERENCES

[1]G. Bao and S. Suresh, Nat. Mater. **2**(11), 715–725 (2003).
[2]A. Mogilner and K. Keren, Curr. Biol. **19**(17), R762–R771 (2009).
[3]D. E. Jaalouk and J. Lammerding, Nat. Rev. Mol. Cell Biol. **10**(1), 63–73 (2009).
[4]J. T. Parsons, A. R. Horwitz, and M. A. Schwartz, Nat. Rev. Mol. Cell Biol. **11**(9), 633–643 (2010).
[5]G. Binnig, C. F. Quate, and C. Gerber, Phys. Rev. Lett. **56**(9), 930–933 (1986).
[6]Y. F. Dufrêne, D. Martínez-Martín, I. Medalsy, D. Alsteens, and D. J. Müller, Nat. Methods **10**, 847–854 (2013).
[7]M. Krieg, G. Fläschner, D. Alsteens, B. M. Gaub, W. H. Roos, G. J. L. Wuite, H. E. Gaub, C. Gerber, Y. F. Dufrêne, and D. J. Müller, Nat. Rev. Phys. **1**(1), 41–57 (2019).
[8]P. K. Hansma, B. Drake, O. Marti, S. A. Gould, and C. B. Prater, Science **243**(4891), 641–643 (1989).
[9]D. Sánchez, N. Johnson, C. Li, P. Novak, J. Rheinlaender, Y. Zhang, U. Anand, P. Anand, J. Gorelik, G. I. Frolenkov, C. Benham, M. Lab, V. P. Ostanin, T. E. Schäffer, D. Klenerman, and Y. E. Korchev, Biophys. J. **95**(6), 3017–3027 (2008).
[10]J. Rheinlaender and T. E. Schäffer, Soft Matter **9**(12), 3230–3236 (2013).
[11]B. B. Akhremitchev and G. C. Walker, Langmuir **15**(17), 5630–5634 (1999).
[12]E. K. Dimitriadis, F. Horkay, J. Maresca, B. Kachar, and R. S. Chadwick, Biophys. J. **82**(5), 2798–2810 (2002).
[13]R. Long, M. S. Hall, M. Wu, and C.-Y. Hui, Biophys. J. **101**(3), 643–650 (2011).
[14]J. A. C. Santos, L. M. Rebelo, A. C. Araujo, E. B. Barros, and J. S. de Sousa, Soft Matter **8**(16), 4441–4448 (2012).
[15]N. Gavara and R. S. Chadwick, Nat. Nanotechnol. **7**(11), 733–736 (2012).
[16]C. F. Draper, D. M. Schaefer, R. J. Colton, and S. M. Hues, in *Forces in Scanning Probe Methods*, edited by H. J. Güntherodt, D. Anselmetti, and E. Meyer (Springer Netherlands, Dordrecht, 1995), pp. 85–90.
[17]M. Pellegrino, M. Pellegrini, P. Orsini, E. Tognoni, C. Ascoli, P. Baschieri, and F. Dinelli, Pflug. Arch. Eur. J. Phy. **464**(3), 307–316 (2012).
[18]J. Rheinlaender and T. E. Schäffer, Anal. Chem. **89**(21), 11875–11880 (2017).
[19]J. Rheinlaender, S. Vogel, J. Seifert, M. Schächtele, O. Borst, F. Lang, M. Gawaz, and T. E. Schäffer, Thromb. Haemost. **113**(2), 305–311 (2015).

[20]W. C. Hayes, L. M. Keer, G. Herrmann, and L. F. Mockros, J. Biomech. **5**(5), 541–551 (1972).
[21]Y. Cao, D. Ma, and D. Raabe, Acta Biomater. **5**(1), 240–248 (2009).
[22]V. Studer, G. Hang, A. Pandolfi, M. Ortiz, W. F. Anderson, and S. R. Quake, J. Appl. Phys. **95**(1), 393–398 (2004).
[23]F. M. Sasoglu, A. J. Bohl, and B. E. Layton, J. Micromech. Microeng. **17**(3), 623–632 (2007).
[24]R. W. Style, R. Boltyanskiy, G. K. German, C. Hyland, C. W. MacMinn, A. F. Mertz, L. A. Wilen, Y. Xu, and E. R. Dufresne, Soft Matter **10**(23), 4047–4055 (2014).
[25]P. D. Garcia and R. Garcia, Biophys. J. **114**(12), 2923–2932 (2018).
[26]M. Zhang, Y. P. Zheng, and A. F. T. Mak, Med. Eng. Phys. **19**(6), 512–517 (1997).
[27]F. Yang, Mech. Mater. **30**(4), 275–286 (1998).
[28]A. M. Korsunsky and A. Constantinescu, Thin Solid Films **517**(17), 4835–4844 (2009).
[29]I. Argatov and G. Mishuris, Mech. Res. Commun. **38**(8), 565–568 (2011).
[30]J. Rheinlaender and T. E. Schäffer, Nanoscale **11**(14), 6982–6989 (2019).
[31]R. W. Clarke, P. Novak, A. Zhukov, E. J. Tyler, M. Cano-Jaimez, A. Drews, O. Richards, K. E. Volynski, C. Bishop, and D. Klenerman, Soft Matter **12**(38), 7953–7958 (2016).
[32]Y. Chen, G. B. Sukhorukov, and P. Novak, Nanoscale **10**(35), 16902–16910 (2018).
[33]D. Thatenhorst, J. Rheinlaender, T. E. Schäffer, I. D. Dietzel, and P. Happel, Anal. Chem. **86**(19), 9838–9845 (2014).
[34]P. Swiatlowska, J. L. Sanchez-Alonso, C. Mansfield, D. Scaini, Y. Korchev, P. Novak, and J. Gorelik, Nanoscale **12**(30), 16315–16329 (2020).
[35]T. E. Schäffer, Anal. Chem **85**(15), 6988–6994 (2013).